Curvature-induced excess surface energy of fullerenes: Density functional theory and Monte Carlo simulations

David Holec,[1,*] Markus A. Hartmann,[2,†] Franz D. Fischer,[3] Franz G. Rammerstorfer,[4] Paul H. Mayrhofer,[1] and Oskar Paris[2]

[1]*Department of Physical Metallurgy and Materials Testing, Montanuniversität Leoben, Franz Josef Straße 18, A-8700 Leoben, Austria*

[2]*Institute of Physics, Montanuniversität Leoben, Franz Josef Straße 18, A-8700 Leoben, Austria*

[3]*Institute of Mechanics, Montanuniversität Leoben, Franz Josef Straße 18, A-8700 Leoben, Austria*

[4]*ILSB, Vienna University of Technology, Gußhausstraße 27-29, A-1040 Vienna, Austria*

(Received 18 March 2010; revised manuscript received 5 May 2010; published 2 June 2010)

Carbon nanostructures are investigated using a multiscale approach based on density functional theory (DFT) and Monte Carlo (MC) simulations. The structure of small fullerenes is calculated using DFT, and simple models are employed to determine classical potential functions which are then used in MC simulations to investigate larger structures. The structural parameters as obtained by DFT and by MC simulations are cross validated for small fullerenes, allowing to understand the effect of the approximations made in MC simulations. It is found that MC overestimates the numerical value of the excess surface energy of carbon nanostructures but the functional dependence, i.e., the decay exponent as a function of the fullerene size, is accurately described. The MC results reveal that bond torsion is the dominant term of the total curvature energy. The combination of DFT and MC allows to get reliable estimates for the excess surface energy of fullerenes as a function of radius for a wide range of fullerene sizes, which may serve as an important input for large-scale finite-element modeling of more complex systems.

DOI: 10.1103/PhysRevB.81.235403 PACS number(s): 81.05.ug, 71.15.Mb, 05.10.Ln

I. INTRODUCTION

Carbon nanostructures are a fascinating class of materials. They include graphene,[1,2] carbon nanotubes,[3,4] and fullerenes[5] but also larger structures such as multiwall nanotubes, carbon onions,[6] and more disordered systems such as carbon fibers.[7] Superior mechanical properties[8,9] as well as tunable electronic properties[10] are only two examples which already find or at least promise many technical applications of such materials in different fields.

The ground state of an infinitely large array of sp^2-bonded carbon is the planar graphene configuration.[1,2] For finite arrays of carbon, the situation changes. The nonsaturated bonds at the edges increase significantly the energy of the system, and bending back and closure of the surface become energetically favorable. The energy per area of such closed surfaces as, e.g., fullerenes and carbon nanotubes is still higher than the energy of (an infinite strip) of graphene. Thus, these structures possess an intrinsic curvature-induced excess surface energy (in the following denoted by *surface energy*), which is an essential input parameter for, e.g., large-scale simulations of mechanical properties of extended carbon nanostructures such as multiwall nanotubes or carbon onions. It is a well-established fact that surface energy and surface stress (see, e.g., Ref. 11 for a distinction between surface energy and surface stress) become increasingly important with decreasing size of objects, in particular, small objects such as nanoparticles. From a continuum mechanical point of view, the existence of a surface stress (which has the same dimension as the surface energy) can be replaced by the action of a normal pressure to the surface, being equivalent to the product of the surface stress and the trace of the curvature tensor (for details see Ref. 11). According to this substitutive normal pressure, an interesting scientific question concerns the (mechanical) stability of carbon onions.[6,12] Besides constitutive physical equations, continuum models that may help to answer this question require quantitative input parameters such as the beforehand mentioned surface energy since curved structures are considered. The literature on fullerenes and nanotubes is extensive; however, investigations on the quantitative description of the surface energy and its dependence on the curvature are scarce. One of the few exceptions is the work of Terrones and Terrones,[13] who calculated the energy of curvature for a series of carbon fullerenes employing a semiempirical Tersoff potential, with the drawback of a wrong C-C bond length. Therefore, the motivation for the investigations presented in this paper is to reinvestigate this area and to provide a reliable estimation of the surface energy as an first approximation to the surface stress of fullerenes and nanotubes.

The method of choice to tackle such a problem is the density functional theory (DFT), which delivers ground-state energies of structures at zero temperature. The smallest fullerene (C_{60}) consists of 60 carbon atoms, and is easily accessible with standard DFT techniques. But fullerene structures consisting of ten thousands of carbon atoms are also possible, and the number of carbon atoms further increases when one considers for instance carbon onions. Due to computational limitations, a full quantum-mechanical description is not possible for such large structures and calls for multiscale modeling approaches. For structures consisting of several ten thousands of atoms Monte Carlo (MC) and molecular dynamics are the appropriate choices. These methods rely on the use of classical potential functions and can be used at any desired temperature.

In this paper, we use DFT calculations to construct classical potentials that are used as input in subsequent MC simulations. The aim is twofold. First, the results of DFT and

MC calculations shall be compared, if possible, to investigate the validity of a classical approach and to understand its possible shortcomings. Second, structures much larger than those accessible with DFT are investigated using MC simulations. Thus, we can extend the range of calculation from C_{240} to C_{5120} and extract—among other interesting information—surface energies for these structures.

The paper is structured as follows. First, we describe calculations employing DFT to investigate the ground state of carbon fullerenes up to C_{240} and also of some single-wall carbon nanotubes (SWNTs). Combining DFT and MC, it is possible to calculate fullerenes up to C_{5120}. In parallel, we investigate also shell structures (see Sec. III B) as a model for ideally spherical fullerenes. In Sec. IV, we first describe how the potentials used in the MC simulations are constructed. Then we present the results on the topology and energy of the fullerenes. The results are discussed with special attention being paid to the comparison of the DFT- and MC-based predictions.

II. METHODS

A. First-principles calculations

The Vienna ab initio simulation package (VASP) (Refs. 14 and 15) with the carbon projector augmented wave pseudopotentials based on the generalized gradient approximation (GGA) employing the Perdew-Burke-Ernzerhof parametrization of the exchange-correlation functional (further referred to as GGA) (Refs. 16 and 17) and ultrasoft local-density approximation (LDA) (further referred to as LDA) pseudopotentials was employed. The **k**-point sampling of $1\times1\times1$ for the fullerenes, $18\times18\times6$ for the graphene two-atom unit cell, and $1\times1\times9$ for the nanotubes were used in order to get the accuracy of around 1 meV/atom. The plane-wave cutoff energy was 400 eV. Vacuum of 8 Å was found sufficient to avoid unphysical interactions between neighboring structures. The same parameters were used also for the ring-shell structures. Since the GGA is known to underestimate bonding while the LDA on the other hand overestimates bonding, using them both will provide a measure for the errors caused by these approximations.

B. Monte Carlo simulations

MC simulations were carried out in the (*NVT*) ensemble (constant number of particles *N*, constant volume *V*, and constant temperature *T*). Following standard MC rules, a displacement of an individual atom was performed with the probability $p=\exp(-\Delta E/k_BT)$,[18,19] where ΔE denotes the difference in the total energy of the system before and after the displacement and k_B is the Boltzmann constant. The calculation of ΔE, which determines the transition probability p in the system, is performed by introducing classical potential functions describing the interactions in the system for any given arrangement of atoms or molecules. The most common approach to describe covalently bonded systems is to approximate the total energy as a sum of two-atom (bond-stretching), three-atom (bond-bending), and four-atom (bond-torsion) contributions. A widely used empirical parameter set employing this concept is realized by the Tersoff-Brenner potential.[20,21]

The approach adopted in this paper is to construct classical potential functions from DFT data, instead of using empirical parameter sets from literature. Thus, a consistent parameter set of classical potentials out of the quantum-mechanical calculations is constructed. Following this strategy, the MC results can be directly compared with the DFT data allowing for a discussion of the quality of the classical potentials and the approximations made during their construction with respect to a full quantum-mechanical treatment. In contrast, if an already existing parameter set was used, it would not be possible to unambiguously attribute differences in the DFT and MC results to the approximations used. The DFT method and the empirical parameter set used would not necessarily have to fit together. Following standard procedures, see, e.g., Refs. 22 and 23, bond-stretching, bond-bending, and bond-torsion terms were included while bond-coupling terms were neglected. Nonlocal (van der Waals) interactions were neglected, too, since they were also not included in the DFT calculations. The expression for the total energy reads

$$E=\sum_{n_1}E^S_{n_1}+\sum_{n_2}E^B_{n_2}+\sum_{n_3}E^T_{n_3} \tag{1}$$

with $E^S_{n_1}$, $E^B_{n_2}$, and $E^T_{n_3}$ being the bond-stretching, bond-bending, and bond-torsion contributions, respectively. The number n_1 spans all bonded pairs of atoms in the system, n_2 and n_3 run over all bond angles and torsion angles in the system, respectively.

The functional form of the bond-stretching term between two bonded atoms i and j is described with the Morse potential,

$$E^S(r_{ij})=E_0(\{1-\exp[\beta(r_{ij}-r_0)]\}^2-1), \tag{2}$$

which is known to describe carbon-carbon bonds better than, e.g., the Lennard-Jones potential. Here r_{ij} and r_0 are the actual and the equilibrium bond lengths, respectively, E_0 the bond energy and β^{-1} the width of the potential.

The bond-bending term is described with a harmonic potential,

$$E^B(\theta_{ijk})=\frac{1}{2}k_\theta(\cos\,\theta_{ijk}-\cos\,\theta_0)^2 \tag{3}$$

with θ_{ijk} being the angle between the i-j and j-k bonds, θ_0 the equilibrium bond angle, and k_θ the bending force constant.

Finally, the torsion contribution is given by the first term in a Fourier series expansion of the torsional potential,[24] which favors a planar arrangement of bonds,

$$E^T(\phi_{ijkl})=\frac{1}{2}k_\phi(1-\cos\,2\phi_{ijkl}). \tag{4}$$

ϕ_{ijkl} is the torsion angle, i.e., the angle between the planes containing atoms $\{i,j,k\}$ and $\{j,k,l\}$ where i-j, j-k, and k-l is a series of successive bonds, k_ϕ is the torsion force constant.

III. TOPOLOGY OF INVESTIGATED STRUCTURES

In order to provide a functional dependence of the total energy on the fullerene size, we had to overcome the main drawback of the DFT calculations, that is, the inability to treat large systems with many atoms. Two approaches were thus considered: (i) a full DFT calculation using approximative structures, which we call "ring shells" and (ii) Monte Carlo simulations using interatomic potentials but treating the complete fullerenes. The classical potentials needed for the application of the MC simulation scheme were obtained by DFT calculations of graphene and carbon SWNTs. All investigated structures have in common that they consist solely of threefold-coordinated (i.e., sp^2-bonded) carbon atoms. In the following paragraphs, we shortly describe the topology of the considered structures.

A. Fullerenes

Euler's formula expresses the relationship between the number of faces (F), edges (E), and corners (C) of closed polyhedral surfaces,

$$2 = C - E + F. \tag{5}$$

Thus, a (closed) three-coordinated structure consisting of only hexagons and pentagons must contain exactly 12 pentagons. An important subclass of these structures is fullerenes with icosahedral symmetry, i.e., the 12 pentagons are isolated from each other and are situated on the corners of a regular icosahedron. These fullerenes can be classified by the specification of two integer numbers, (m,n), describing the mutual position of two neighboring pentagons. The number of corners is then $C=20(m^2+mn+n^2)$.[25] In this paper, we consider icosahedral fullerenes of type $(0,n)$ with n ranging up to 16 corresponding to a fullerene with 5120 carbon atoms. The only two exceptions are C_{60} [(1, 1) type] and C_{240} [(2, 2) type]. The initial structures were built using a layer-by-layer assembly of a planar graph,[26,27] which was subsequently projected on a perfect sphere. Using a DFT full shape relaxation with the quasi-Newton residual minimization method, direct inversion in the iterative subspace algorithm[28] or a MC equilibration procedure, these structures were relaxed to their ground states and further investigated.

B. Ring shells

A severe limitation of DFT calculations is the rapidly increasing computational time needed for large systems. A full DFT treatment was therefore applied only for fullerenes up to C_{240}. To evaluate the influence of larger radii of curvature on the surface energy, large fullerenes were approximated with a spherical segment consisting of several hexagonal carbon rings. The broken C-C bonds were saturated with hydrogen atoms (see Fig. 1). The energies calculated for these structures were used to estimate the surface energy of large fullerenes with radii corresponding to those of the shells. In particular, we used a one-ring shell (12 atoms in total, six C atoms in a hexagonal ring and six dangling bond saturated with 6 H atoms), a two-ring shell (in total 24 atoms, 12 C atoms in two rings and 12 H atoms saturating the broken bonds), and a three-ring shell (36 atoms in total, 24 C atoms and 12 H atoms). This approximation relies on the following assumptions: (i) a fullerene can be approximated with a sphere, (ii) the surface of large fullerenes consists mainly of hexagons (the number of 12 pentagons is fixed for all sizes), and (iii) the broken C-C bonds can be "saturated" with H atoms (with a fixed C-H bond length) without disturbing the characteristics of the carbon bonds. The C-C bond length was kept at the value corresponding to the equilibrium graphene value ($b_{\text{C-C}}^{\text{GGA}}=1.4263$ Å, $b_{\text{C-C}}^{\text{LDA}}=1.4119$ Å). Subsequently, the C-H bond length was optimized in order to get the best fit of energy per area to the ideal graphene. This procedure yielded $b^{\text{C-H}}=1.09$ Å for the one-ring shell, $b^{\text{C-H}}=1.08$ Å for the two-ring shell, and $b^{\text{C-H}}=1.09$ Å for the three-ring shell structure using the LDA. Using the GGA, two optimum C-H bond lengths were obtained for the one- and three-ring shells: $b^{\text{C-H}}=0.96$ Å and $b^{\text{C-H}}=1.26$ Å for the one-ring shell, $b^{\text{C-H}}=1.08$ Å for the two-ring shell, and $b^{\text{C-H}}=0.97$ Å and $b^{\text{C-H}}=1.25$ Å for the three-ring shell structure. The energies for the one- and three-ring shells are almost independent which of the two optimum bond lengths is used. The ring-shell structures with various radii were obtained by projecting the planar ring patterns on spheres with the corresponding radii while keeping all the bond lengths constant.

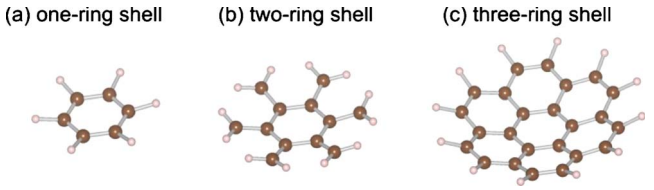

FIG. 1. (Color online) The shell models: (a) one-ring, (b) two-ring, and (c) three-ring shells. Small balls represent hydrogen atoms passivating the broken C-C bonds (see text for explanation).

C. Nanotubes

SWNTs were primarily used to determine the torsion part of the potentials used for the MC simulations (see Sec. II B) and the surface energy as a function of their radius was obtained as a side product. SWNTs of armchair (n,n) and zigzag $(n,0)$ type were investigated,[29] as these two types correspond to the two extreme cases of how a graphene sheet may fold into a SWNT. In turn, we have obtained two different estimates for the torsion constants (see Sec. IV A).

IV. RESULTS

A. MC potentials from DFT calculations

DFT data were used to obtain the unknown force constants in the above-described potential functions [Eqs. (2)–(4)]. Isotropic homogenous in-plane stretch deformation, i.e., the same magnitude in all directions, was applied to a graphene sheet, and the resulting energy vs bond-length data points were fitted with Eq. (2) (see Fig. 2). This procedure yielded $E_0=6.1322$ eV, $\beta=1.8502$ Å^{-1}, and $r_0=1.4322$ Å using GGA while LDA gave $E_0=6.7104$ eV, β

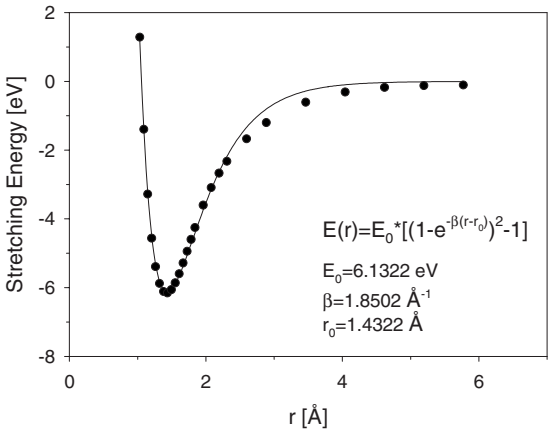

FIG. 2. Stretching energy per bond vs the bond-length GGA DFT data points together with the bond-stretching potential as used for the MC calculations.

$=1.8504$ Å^{-1}, and $r_0=1.4169$ Å. The Morse potential fits the data remarkably well whereas the Lennard-Jones potential is not able to reproduce the functional dependence adequately.

Two different deformation modes were used to obtain the force constants for bending: (i) uniaxial stretching and (ii) shear deformation [Figs. 3(a) and 3(b)], respectively. The right side of Fig. 3 shows the deformations applied for the uniaxial and shear deformation, respectively. In the uniaxial stretching mode, the graphene sheet was stretched only in the y direction. As a consequence, only the bond angles (and not the bond lengths) change. There are two different angles in the deformed unit cell: θ and $(180°-\theta/2)$. Symmetry dictates the equilibrium angle to be $\theta_0=120°$. The GGA calculated data points yield $k_\theta^{(1)}=9.08$ eV (and $k_\theta^{(1)}=8.7$ eV for the corresponding LDA calculations). In contrast to the uniaxial stretching mode, both the angles and the bond lengths change in the shear deformation mode [see Fig. 3(b)]. Assuming that the total energy of the system is a simple sum of the different energy terms, the bond-stretching contribution (now known) can be subtracted and once again we should obtain the energy purely due to bond bending. Doing so, one finds for the GGA data points $k_\theta^{(2)}=10.84$ eV (the corresponding LDA value is $k_\theta^{(2)}=11.46$ eV). The fact that $k_\theta^{(1)}\neq k_\theta^{(2)}$ is a first indication that splitting the total energy into a sum of different contributions is not exactly valid but it is only an approximation.

Carbon nanotubes of different diameters and geometries were used to obtain the torsion constant. Figure 4 shows the torsion energy together with the fitted linear dependence for an extraction of the torsion constant. Using $k_\theta=(k_\theta^{(1)}+k_\theta^{(2)})/2\approx 10$ eV for the bending force constant, a torsion constant $k_\phi=0.346$ eV ($k_\phi=0.397$ eV for the LDA calcula-

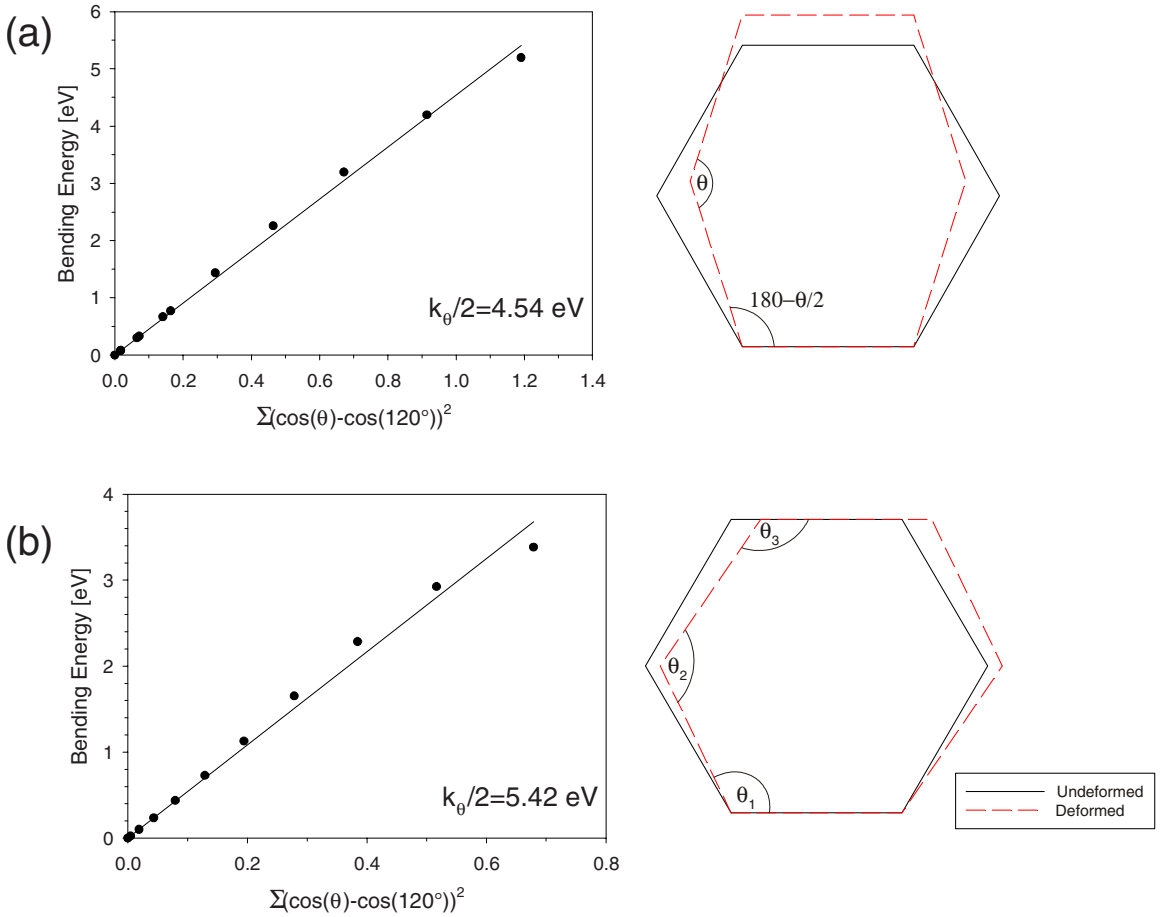

FIG. 3. (Color online) (a) The uniaxial stretching and (b) the shear deformation modes were used to obtain the bond-bending force constants (left side, GGA data points). The corresponding deformation modes are schematically presented on the right side.

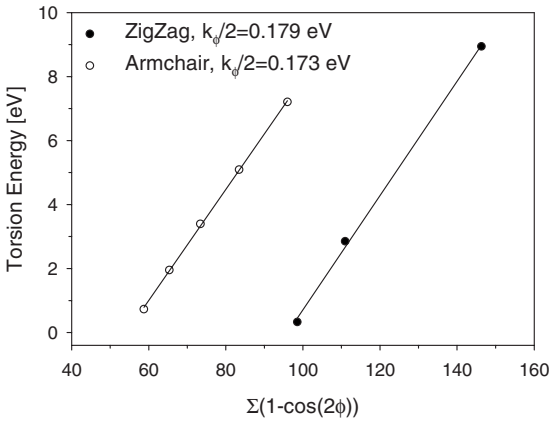

FIG. 4. The torsion contribution to the total energy as obtained from the armchair and zigzag SWNTs GGA data sets.

tions) was obtained almost independent on the different geometries (armchair and zigzag SWNTs). Although the data points could be perfectly fitted with the assumed functional form of the torsion potential, the fact that the torsion energy shows a significant negative offset (instead of passing through the origin) as well as that the energy curves show a horizontal shift for the two different geometries points once again toward the approximative form of the interatomic potentials being used.

Table I summarizes the obtained force constants used further on for the MC simulations of the fullerenes.

B. Geometry of fullerenes

Basic characteristics of the optimized fullerenes as obtained from the DFT and the MC simulations are summarized in Table II. The apparent radii r of the fullerenes were calculated according to the following definition,

$$r = \langle |\mathbf{r}_i - \mathbf{R}| \rangle, \tag{6}$$

where $\mathbf{r}_i$ is the position vector of the ith atom, $\mathbf{R}$ is the position vector of the center of mass of the fullerene, and angular brackets denote averaging over all atoms. Only four fullerenes, C_{60}, C_{70}, C_{180}, and C_{240}, were calculated using DFT; results for larger structures up to C_{5120} come solely from MC simulations. While the DFT calculations were carried out at zero temperature, the temperature in the MC simulations was set according to $k_BT=25$ μeV, i.e., 0.1% of the energy corresponding to room temperature. The finite temperature was chosen to avoid computational problems such as trapping in local minima. A temperature of 25 μeV is large enough to avoid these problems but also small enough that the system is found essentially in its global energy minimum without any additional entropy effect (note that in a MC simulation it is the free energy that is minimized not the internal energy). Figure 5 shows snapshots of four representative structures optimized with the MC method. The overall shape of the fullerenes from DFT and MC methods is the same and agrees well with previous studies in the literature.[30,31] The C_{60} atoms lie on a sphere. With increasing number of carbon atoms, the regions with only hexagons become flatter while pronounced vertices are formed near the pentagons. This flattening is clearly shown by both the DFT and MC calculations. Since graphene has a lower energy per bond than any curved fullerene, the tendency for faceting may be seen as an effort to minimize the total energy by becoming more similar to graphene in the hexagon regions on the expense of forming vertices around the pentagons.

TABLE I. Parameters of the constructed classical potentials for the MC calculations. E_0, β, and r_0 are related to the bond-stretching term, k_θ and θ_0 describe the bond-bending contribution, and k_ϕ is the torsion force constant. The two data sets (GGA and LDA) correspond to the two different DFT pseudopotentials considered.

Quantity	GGA	LDA
E_0	6.1322 eV	6.7104 eV
β	1.8502 Å^{-1}	1.8054 Å^{-1}
r_0	1.4322 Å	1.4169 Å
k_θ	10 eV	10 eV
θ_0	120°	120°
k_ϕ	0.346 eV	0.397 eV

Figure 6 presents the bond lengths histograms for C_{60}, C_{240}, C_{320}, and C_{2000}. A comparison of DFT and MC results reveals an interesting behavior. For the smallest fullerene, C_{60}, the bond lengths histograms obtained with the two methods match perfectly. The distribution shows a single peak centered at the equilibrium bond length. The only difference is the height (and the width) of the distribution, which is smaller (larger) in the case of the MC simulations. This stems from the fact that in contrast to the DFT calculations the MC simulations were not performed at exactly zero temperature, which leads to the broadening of the infinitely sharp distribution at zero temperature (the small broadening of the DFT simulation results from a numerical noise, i.e., the accuracy used). The single peak splits into four distinct peaks for the C_{240} fullerene, which is reflected by both the DFT as well as the MC simulations. In this case, the positions of the four peaks are different for the two calculations: the DFT results are shifted to slightly lower bond lengths; the larger the fullerenes the larger the width of the peaks, see, for example, C_{320} and C_{2000} in Fig. 6. The C_{2000} exhibits only one large (flat facets) and only some smaller side peaks (vertices around pentagons).

C. Excess surface energy

An important outcome of this work with respect to large-scale continuum modeling is the surface energy as a function of the fullerene radius (i.e., its size). We define the (excess) surface energy of a fullerene as the increase in its total energy with respect to (planar) graphene. Consequently, the presented surface energy is a quantity averaged over the whole surface of a fullerene. It is beyond the scope of this paper to give a position-dependent surface energy reflecting the local curvature. Unless stated otherwise, the surface energy is expressed *per bond*.

TABLE II. Radii and curvature energies for the fullerenes considered in this study calculated using the DFT and MC methods. The surface energy is the difference between the energy per bond of the structurally optimized fullerene and graphene (i.e., the parameter E_0 of the bond-stretching potential). The radius was calculated as the mean distance between the center of mass and all atoms forming a fullerene. Literature data (Ref. 30) for radii from a GGA-based study are labeled with a star (*).

	DFT				MC			
	GGA		LDA		GGA		LDA	
	r (Å)	ΔE (eV/bond)	r (Å)	ΔE (eV/bond)	r (Å)	ΔE (eV/bond)	r (Å)	ΔE (eV/bond)
C_{60}	3.55	0.253	3.52	0.259	3.55	0.397	3.51	0.434
	3.55*							
C_{70}	3.84	0.225	3.80	0.231				
C_{180}	6.16	0.117	6.08	0.119	6.16	0.184	6.10	0.201
	6.13*							
C_{240}	7.08	0.091			7.11	0.150	7.04	0.164
	7.07*							
C_{320}					8.20	0.125	8.12	0.137
C_{500}					10.23	0.092	10.13	0.101
C_{720}					12.26	0.071	12.13	0.078
C_{980}					14.28	0.056	14.14	0.062
C_{1280}					16.31	0.046	16.14	0.051
C_{1620}					18.34	0.038	18.15	0.042
C_{2000}					20.37	0.032	20.15	0.036
C_{2880}					24.42	0.024	24.17	0.027
C_{5120}					32.54	0.015	32.20	0.017

Figure 7 shows the surface energy as calculated with the three different approaches described in this paper: DFT full structures (circles) and MC full structures (squares) in Fig. 7(b), and the ring shells in Fig. 7(c). Using DFT for the full fullerene structures it was possible to calculate the energy only up to C_{240}, i.e., a radius of ≈ 7 Å. The MC approach was applied to fullerenes up to C_{5120} corresponding to a radius of more than 30 Å. The ring-shell approximation can, in principle, access any radius (calculated up to 500 Å). All three data sets could be reasonably well fitted with a power law of the form

$$E \propto r^{\beta} \tag{7}$$

with $\beta=-1.43$ for the DFT full structures (correlation coefficient $R^2=0.9996$) and $\beta=-1.40$ for the MC simulations ($R^2=0.9985$), respectively (in all three cases, the β exponents were obtained by fitting the LDA and GGA data sets together). Different values are obtained for the ring-shell models fitted to the entire data range: $\beta=-2.30$ for one-ring shells, $\beta=-2.64$ for the two-ring shell model ($R^2=0.9997$), and $\beta=-4.05$ for the three-ring shells. It is interesting to note that even though C_{70} does not have the icosahedral symmetry, its surface energy falls nicely onto the trend of the icosahedral fullerenes [see Fig. 7(b)].

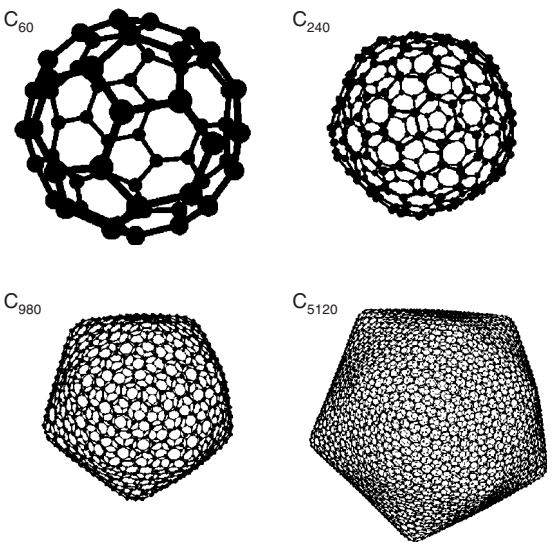

FIG. 5. Snapshots of four fullerenes as optimized using MC. The large area flat facets are being formed already for the C_{980}.

The approximations made during constructing the MC potentials lead to an overestimation of the absolute values of the surface energy by a factor of ≈ 1.57. However, the exponent β differs by only $\approx 2\%$ with respect to the one coming from the DFT fullerene calculations. On the other hand, the ring-shell models strongly overestimate the exponent which is most likely caused by an inappropriate representation of the fullerene geometry. In particular, (i) the large fullerenes approximated as ring shells do not show the correct bond lengths and shape (spherical vs faceted) and (ii) the ring shells, in fact, approximate structures consisting only of

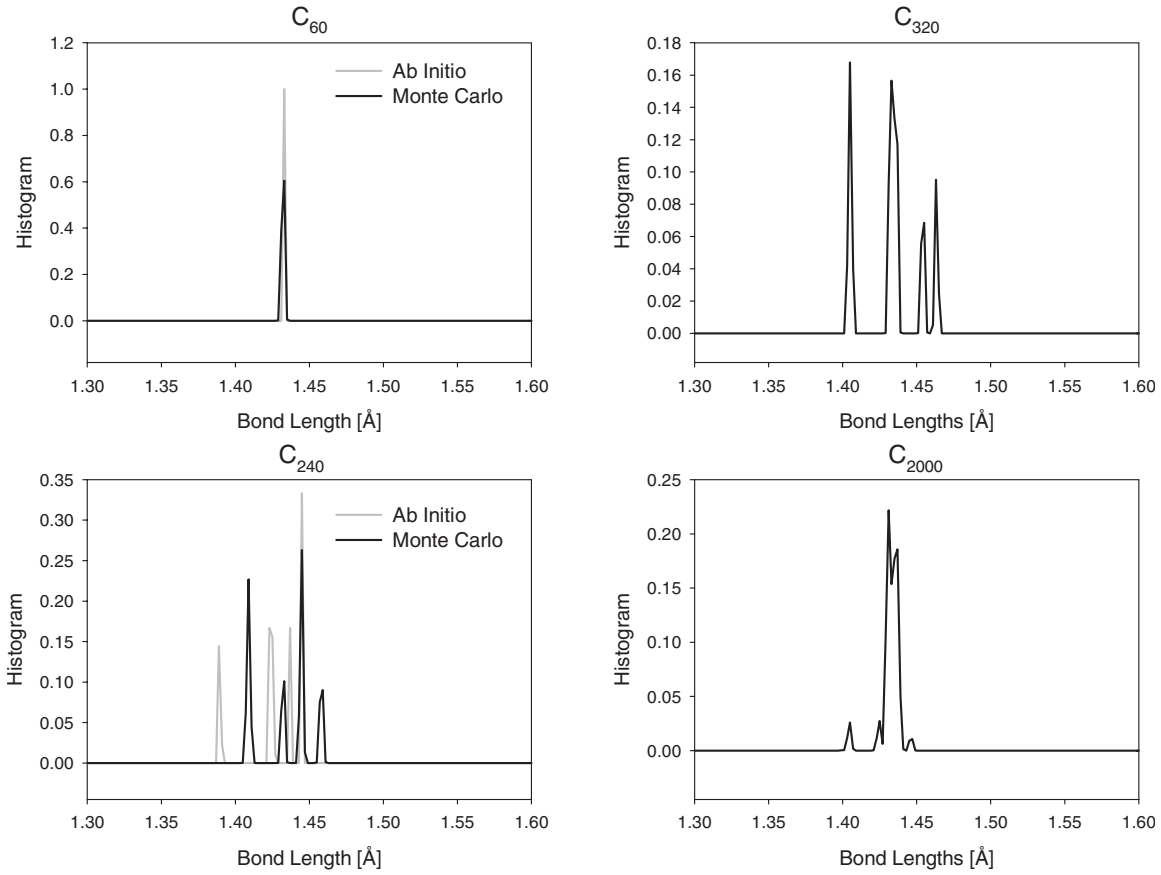

FIG. 6. Bond-length histograms for four fullerenes. The gray lines shown for C_{60} and C_{240} represent the DFT data. The large wide peak for the C_{2000} corresponds to the relatively flat facets composed of only hexagons.

hexagons and no pentagons. This fact is clearly demonstrated in Figs. 7(b) and 7(c) for small radii where the discrepancy between the ring-shell and the DFT full structure data points is significant (e.g., for $r=3$ Å, the two-ring shell having no pentagon is projected on almost a half of the corresponding sphere while half of the C_{60} with $r\approx 3.5$ Å contains six pentagons).

While DFT gives only the total energy, in MC simulations various contributions to the total energy are explicitly calculated. Figure 8 shows the contributions from stretching, bending, and torsion deformations. Each of them individually follows a power-law dependence on the radius but with different exponents: $\beta=-2.18$ for stretching, $\beta=-1.80$ for bending, and $\beta=-1.33$ for torsion, respectively. The stretch-

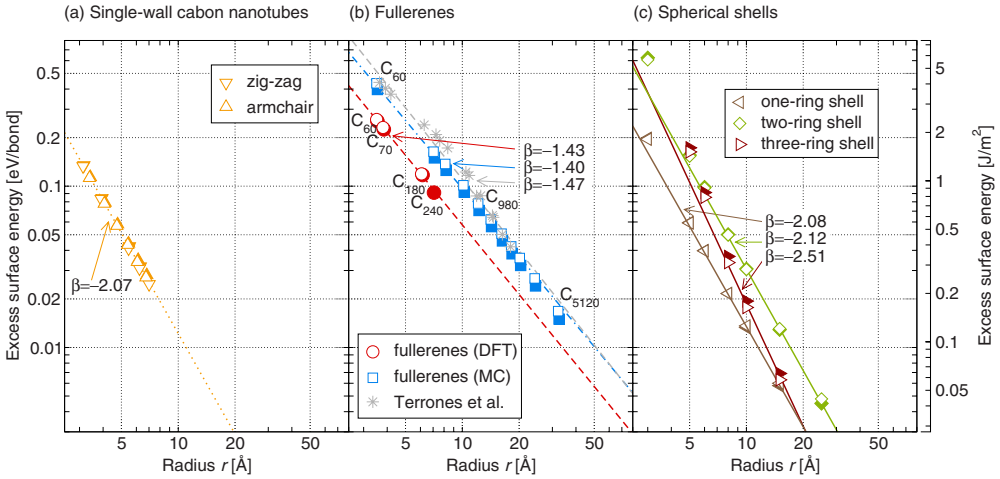

FIG. 7. (Color online) Double logarithmic plot of surface energy vs radius: (a) the zigzag (down triangle) and armchair (up triangle) SWNTs from the DFT calculations, (b) fullerenes as calculated by DFT (circles) and the MC (squares) using the full structures, and (c) the ring-shell models fitted for data with $r>10$ Å. The full (open) symbols correspond to the GGA (LDA) approximations. Data from the literature in (b) are included for comparison (Ref. 13).

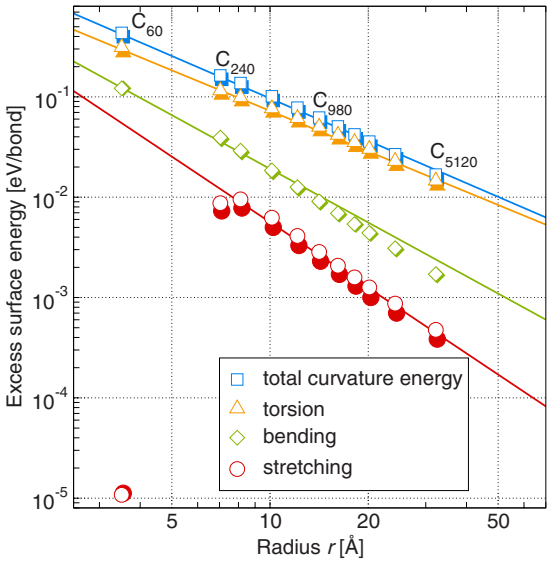

FIG. 8. (Color online) Double logarithmic plot of stretching, bending, and torsion contributions to the surface energy obtained from the MC calculations. The full (open) symbols correspond to the GGA (LDA) based potentials.

ing contribution is the only to show nonmonotonic behavior. For C_{60}, the stretching part is almost zero, as is expected, since all the bond lengths are centered at the equilibrium bond length (see Fig. 6). The splitting of the peak of bond lengths leads to an increased energy that reaches a maximum for C_{240}. The given exponent describes the decay after the maximum. An interesting observation is that torsion gives the largest contribution (with the slowest decay) to the total energy, although the torsion force constant is by far the smallest.

As mentioned in Sec. I, the motivation for this study was to estimate the surface energy of carbon fullerenes, i.e., the energy per unit area. However, isolated fullerenes are actually not spheres, in contrast to what seems so be the case for multilayered "onion" structures.[6,12,13] Therefore, it is quite difficult to extract the surface energy as a function of the radius. For spherical layers of carbon onions, the ring-shell models become more appropriate due to the correct geometry. Focusing only on structures with $r > 10$ Å, where large areas consisting only of hexagons are present, following decay parameters (identical for both, energy per bond and energy per area dependencies) are obtained: $\beta = -2.08$ for one-, $\beta = -2.12$ for two-, and $\beta = -2.51$ for three-ring shells [see Fig. 7(c)]. Since a larger shell model (i.e., modeling a larger portion of the spherical surface) is likely to be less influenced by inaccuracies caused by the dangling bonds, $\beta \approx -2.5$ is the best estimate for the decay parameter of spherical fullerenes based on the present calculations.

Having calculated the DFT energies of SWNTs for the estimation of the torsion force constant, we can estimate the β exponent also for these objects. SWNTs have two different curvatures in the two perpendicular directions (zero curvature along the SWNTs' axis) which distinguish them from spherical fullerenes having a (more or less) uniform curvature. The results plotted in Fig. 7 clearly show that the data points from both extreme SWNTs types, the zigzag and armchair types, follow the same power law with $\beta = -2.07$ (energy per bond dependence). The calculated SWNTs radii are in excellent agreement with the values from the literature.[29,32] In this case, the actual surface can be approximated with much higher reliability than for the fullerenes yielding $\beta = -2.04$ for the energy per area dependence.

V. DISCUSSION

In this paper, fullerenes up to C_{240} were studied using DFT methods while different approximations were applied to investigate larger structures. As long as isolated fullerenes were considered, an attempt to approximate large fullerenes with parts of spherical surfaces (ring shells) yielded unsatisfactory results. However, it should be mentioned that the results obtained from the ring-shell model might be of some value for estimating the surface energy of the individual layers of carbon onions, which form rather perfect spheres even for a very large number of atoms. In particular, for larger spherical layers of carbon onions, the influence of the 12 pentagons diminishes and so does the error caused by neglecting them in the model.

A different approximation is achieved by switching from a full quantum-mechanical description to MC simulations that still keep the discrete nature of matter but describe the interactions between atoms with classical potentials. This intermediate step is needed to calculate relevant physical parameters which can subsequently be used as input parameters for continuum models, e.g., finite-element calculations. In this paper, we have made the first step: DFT calculations were used to construct interatomic potentials between carbon atoms. These potentials were used in MC simulations of fullerene structures with increasing size. The two methods were cross validated where possible.

Energy contributions from two- (stretching), three- (bending), and four-body (torsion) interactions were included. Two different deformation modes were used for estimation of the bond-bending potential. In an ideal case, both should lead to the same results. Since this was not the case, obviously splitting of total energy into a simple sum of individual contributions is not exact. In other words, the energy contributions due to stretching, bending, and torsion are not completely independent. It is argued in literature that also the coupling terms, e.g., bond stretching-bending or stretching-torsion, as well as nonbonded terms (van der Waals interactions) have to be included.[33] Although these terms were neglected in the present work, the results obtained give a reliable estimate for the purposes of subsequent macroscopic simulations while keeping the extremely simple form of the potentials (and thus the MC calculations are highly affordable).

A comparison of DFT and MC results reveals that MC predicts higher excess curvature energies. Using the fitted power laws, we find that the MC simulations overestimate the energy by a factor of ≈ 1.57. A similar result is obtained also from a comparison with the work of Ref. 13, where the Tersoff potential[34,35] was used (see Fig. 7). This overestimation stems from the fact that the potentials for stretching as well as for bending were calculated for graphene, which is a planar configuration, and then used for the curved configu-

ration of fullerenes. If, for example, we take the C_{60} fullerene, keep all the atoms fixed and only change the bond length (i.e., alter the stretching part while keeping bending and torsion contributions constant), we obtain slightly different parameters for the stretching potential. Additionally, the energy values obtained for the planar configuration are higher than for the curved fullerenes (cf. Fig. 4), which is demonstrated by the strong negative offset. These effects can probably be compensated by considering bond coupling terms as suggested in Ref. 33, where negative values for the stretching-torsion coupling constant are found, which would lower the total energy of our systems. The quantum-mechanical origins of these difficulties lie in the complexity of the electronic cloud around the nuclei. While the charge distribution above and below the graphene plane is symmetric, there is about 20% less charge accumulated inside than outside the C_{60} sphere. Consequently, the interatomic interactions within the curved surfaces are inherently more complex than in the planar structures implying that even the stretching potential should not be expected to be transferable from the planar to the curved surface. Nevertheless, although the absolute values of the energy are overestimated by the MC method, both methods yield almost the same exponent β for the size dependence of the surface energy, which demonstrates that the functional dependence of the energy on the radius is the same.

The DFT and MC simulations have resulted in the same relaxed structures. While the distribution of bond lengths has a single peak for C_{60}, it splits into several peaks for larger fullerenes. The splitting is correctly reproduced by the MC method (e.g., four peaks with similar spacing are obtained for both, MC and DFT, calculations) whereas the positions of the single peaks from the MC calculations are slightly shifted with respect to the DFT results. Similar bond-length distributions were reported earlier by other groups,[31] although their histograms seem to be sharper (C_{320} being the exception). We ascribe this discrepancy to different tools used for the structure optimizations. It is worth pointing out that in the MC simulations the splitting is observed only when the torsion contributions, i.e., four-particle interactions, are taken into account. If only stretching and bending terms are considered, no splitting occurs, suggesting that the four-particle interactions are essential for the correct description of fullerenes. Furthermore, torsion yields by far the highest contribution to the surface energy albeit the small force constant. We attribute this to the fact that, in contrast to the bond length and angle, the torsion angle cannot be kept close to its equilibrium value in a curved geometry (geometric frustration). The stretching contribution can be kept small by ensuring the bond lengths being close to their equilibrium values, and also the bending part can be reasonably minimized (only the 12 pentagons show bending angles of $\approx 108°$). In contrast, the torsion contribution that favors a planar configuration cannot be eliminated. In fact, one may be tempted to assume that the torsion contribution can be minimized by maximizing the radius of the fullerene since a large radius approximates the planar graphene layer best. This reasoning is, however, not correct. A simple rescaling of the coordinates of all the atoms present in the structure leaves the torsion contribution unaltered, as one can easily see in the definition of the torsional angles. The planar state is approximated only, if the radius as well as the number of atoms in the structure increase. Nevertheless, considering the almost parallel slope of MC and DFT data in Fig. 7, it seems unlikely that higher-order contributions (five particle and more) to the potential energy play a significant role, although they might change the absolute values of the energy.

VI. CONCLUSIONS

Geometry and energy of carbon fullerenes were studied by a combination of density functional theory and Monte Carlo methods. DFT was used to construct compatible MC potentials which were subsequently used for studies of large fullerenes that cannot be easily handled by the standard DFT tools. The (curvature induced excess) surface energy follows a power law as a function of the structure mean radius. Both methods used yielded practically the same power-law exponent for the surface energy per bond: $\beta^{\mathrm{DFT}}=-1.43$ and $\beta^{\mathrm{MC}}=-1.40$. When the surface energy is expressed per area, the exponents change to $\beta^{\mathrm{DFT}}=-1.67$ and $\beta^{\mathrm{MC}}=-1.40$. The fullerenes do not have spherical shape which is in contradiction with experimental observations in onion structures. We therefore modeled perfect spherical structures using approximative shell models which yielded $\beta\approx-2.5$ for the energy per area function.

Classical MC potentials for the sp^2-bonded carbon were constructed based on the DFT data in order to obtain compatible data sets. A detailed discussion on their performance with respect to the full quantum-mechanical description was given. It has turned out that only stretching (two-particle) and bending (three-particle) interactions are not able to reproduce the correct fullerene geometries (i.e., bond-length and angle distributions leading to extended flattened areas), for which at least the four-particle interaction (i.e., torsion) has to be included.

ACKNOWLEDGMENTS

Financial support by the START Program (Y371) of the Austrian Science Fund (FWF) is greatly acknowledged. F.D.F. thanks D. Vollath, Karlsruhe, Germany, for the motivation to do this research and for extensive discussions.

*david.holec@unileoben.ac.at
†markus.hartmann@unileoben.ac.at

[1] K. S. Novoselov, A. K. Geim, S. V. Morozov, D. Jiang, Y. Zhang, S. V. Dubonos, I. V. Grigorieva, and A. A. Firsov, Science **306**, 666 (2004).
[2] K. S. Novoselov, D. Jiang, F. Schedin, T. J. Booth, V. V. Khotkevich, S. V. Morozov, and A. K. Geim, Proc. Natl. Acad. Sci. U.S.A. **102**, 10451 (2005).
[3] D. S. Bethune, C. H. Klang, M. S. de Vries, G. Gorman, R. Savoy, J. Vazquez, and R. Beyers, Nature (London) **363**, 605 (1993).
[4] S. Iijima and T. Ichihashi, Nature (London) **363**, 603 (1993).
[5] H. W. Kroto, J. R. Heath, S. C. O'Brien, R. F. Curl, and R. E. Smalley, Nature (London) **318**, 162 (1985).
[6] F. Banhart and P. M. Ajayan, Nature (London) **382**, 433 (1996).
[7] O. Paris and H. Peterlik, in *Handbook of Textile Fibre Structure*, edited by S. Eichhorn, J. W. S. Hearle, M. Jaffe, and T. Kikutani (Woodhead, Oxford, 2009), Vol. 2, p. 353.
[8] O. Lourie, D. M. Cox, and H. D. Wagner, Phys. Rev. Lett. **81**, 1638 (1998).
[9] D. Loidl, O. Paris, M. Burghammer, C. Riekel, and H. Peterlik, Phys. Rev. Lett. **95**, 225501 (2005).
[10] X. Jia *et al.*, Science **323**, 1701 (2009).
[11] F. D. Fischer, T. Waitz, D. Vollath, and N. K. Simha, Prog. Mater. Sci. **53**, 481 (2008).
[12] F. Banhart, T. Füller, P. Redlich, and P. M. Ajayan, Chem. Phys. Lett. **269**, 349 (1997).
[13] H. Terrones and M. Terrones, J. Phys. Chem. Solids **58**, 1789 (1997).
[14] G. Kresse and J. Furthmüller, Phys. Rev. B **54**, 11169 (1996).
[15] G. Kresse and J. Hafner, Phys. Rev. B **47**, 558 (1993).
[16] G. Kresse and D. Joubert, Phys. Rev. B **59**, 1758 (1999).
[17] J. P. Perdew, K. Burke, and M. Ernzerhof, Phys. Rev. Lett. **77**, 3865 (1996).
[18] K. Binder, Rep. Prog. Phys. **60**, 487 (1997).
[19] K. Binder and D. W. Heermann, *Monte Carlo Simulation in Statistical Physics*, Springer Series in Solid-State Sciences, 4th ed. (Springer, New York, 2002).
[20] D. W. Brenner, Phys. Rev. B **42**, 9458 (1990).
[21] D. W. Brenner, O. A. Shenderova, J. A. Harrison, S. J. Stuart, B. Ni, and S. B. Sinnott, J. Phys.: Condens. Matter **14**, 783 (2002).
[22] J. H. Walther, R. Jaffe, T. Halicioglu, and P. Koumoutsakos, J. Phys. Chem. B **105**, 9980 (2001).
[23] X. Hao, H. Qiang, and Y. Xiaohu, Compos. Sci. Technol. **68**, 1809 (2008).
[24] J. C. Sancho-García, A. J. Pérez-Jiménez, J. M. Pérez-Jordá, and F. Moscardó, Chem. Phys. Lett. **342**, 452 (2001).
[25] A. Šiber, Phys. Rev. E **73**, 061915 (2006).
[26] P. W. Fowler, D. E. Manolopoulos, D. B. Redmond, and R. P. Ryan, Chem. Phys. Lett. **202**, 371 (1993).
[27] P. W. Fowler and K. M. Rogers, J. Chem. Inf. Comput. Sci. **41**, 108 (2001).
[28] P. Pulay, Chem. Phys. Lett. **73**, 393 (1980).
[29] S. Niyogi, M. A. Hamon, H. Hu, B. Zhao, P. Bhowmik, R. Sen, M. E. Itkis, and R. C. Haddon, Acc. Chem. Res. **35**, 1105 (2002).
[30] R. R. Zope, T. Baruah, M. R. Pederson, and B. I. Dunlap, Phys. Rev. B **77**, 115452 (2008).
[31] P. Calaminici, G. Geudtner, and A. M. Köster, J. Chem. Theory Comput. **5**, 29 (2009).
[32] V. Jindal and A. N. Imtani, Comput. Mater. Sci. **44**, 156 (2008).
[33] J. R. Maple, M.-J. Hwang, T. P. Stockfisch, U. Dinur, M. Waldman, C. S. Ewig, and A. T. Hagler, J. Comput. Chem. **15**, 162 (1994).
[34] J. Tersoff, Phys. Rev. Lett. **61**, 2879 (1988).
[35] J. Tersoff, Phys. Rev. B **37**, 6991 (1988).